

ENGINEERING

Rapid, continuous additive manufacturing by volumetric polymerization inhibition patterning

Martin P. de Beer^{1*}, Harry L. van der Laan^{2*}, Megan A. Cole¹, Riley J. Whelan¹, Mark A. Burns^{1,3†}, Timothy F. Scott^{1,2†}

Contemporary, layer-wise additive manufacturing approaches afford sluggish object fabrication rates and often yield parts with ridged surfaces; in contrast, continuous stereolithographic printing overcomes the layer-wise operation of conventional devices, greatly increasing achievable print speeds and generating objects with smooth surfaces. We demonstrate a novel method for rapid and continuous stereolithographic additive manufacturing by using two-color irradiation of (meth)acrylate resin formulations containing complementary photoinitiator and photoinhibitor species. In this approach, photopatterned polymerization inhibition volumes generated by irradiation at one wavelength spatially confine the region photopolymerized by a second concurrent irradiation wavelength. Moreover, the inhibition volumes created using this method enable localized control of the polymerized region thickness to effect single-exposure, topographical patterning.

INTRODUCTION

Additive manufacturing (AM) methods enable facile fabrication of exceptionally complex objects with internal features unobtainable by conventional methods (1). Commonly called three-dimensional (3D) printing, these technologies typically produce 3D structures by successive addition of thin layers of material. The simple operation and near limitless design choice have made AM very attractive for producing custom and prototype parts (2), finding utility in applications ranging from the fabrication of bespoke medical devices (3–5) and athletic equipment tailored to an individual's anatomy (6) to the low volume production of automotive and aerospace components (7). A wide variety of materials, including thermoplastics, polymeric resins, and inorganic powders, have been used as AM media for methods ranging from material extrusion (8–10) to powder bed fusion (11) and binder jetting (12). A particular method of interest, stereolithographic AM (SLA) (13, 14), uses photopolymerizable resin and a patterned illumination source to cure cross-sectional layers of the desired geometry. The speed of many layer-by-layer SLA devices is, depending on the build platform translation direction, limited by either adhesion of cured polymer to the projection window or resin surface disturbances, necessitating time-consuming separation or recoating steps between successive layers. Consequently, the print speeds in these systems range from only a few millimeters to several centimeters per hour. The recently described continuous liquid interface production technique (15–17) addresses this deficiency by using an oxygen-permeable projection window to create a thin, polymerization-free resin layer adjacent to the projection window, enabling continuous part production at translation speeds of several hundred millimeters per hour. Nevertheless, contemporary AM systems are ill suited for the production of arbitrary 3D objects without movement of the build platform.

We have developed an AM system that can print continuously at relatively high linear velocities in addition to printing 3D structures using a single exposure. Our process, shown in Fig. 1A, uses a build head that is drawn upward out of a photopolymerizable resin and two illu-

mination sources at different wavelengths. Patterned illumination from below through a transparent glass window initiates polymerization of the resin, while illumination at a second wavelength inhibits the polymerization reaction immediately adjacent to the glass window, eliminating adhesion and enabling continuous operation. Print speeds of approximately 2 m/hour have been achieved, and the process is compatible with a wide variety of resins including acrylates, methacrylates, and vinyl ethers. In addition, by varying the intensity of the light source on a per-pixel basis, the system can perform surface topographical patterning in a single exposure/layer with no stage translation.

RESULTS

Dual-wavelength volumetric photopolymerization confinement

A unique aspect of our system is the use of a multicolor system to achieve volumetric patterning by the photochemical generation of both polymerization initiation and polymerization inhibition species. Common among all contemporary SLA devices is the use of a single wavelength of light to initiate polymerization patterned in a plane. In contrast, we use one wavelength to photochemically activate polymerization and a second wavelength to inhibit that reaction. Here, photopolymerizable resins are formulated with camphorquinone (CQ; Fig. 1B) and ethyl 4-(dimethylamino)benzoate (EDAB; Fig. 1C) as a visible light photoinitiator and co-initiator, respectively (18), and bis[2-(*o*-chlorophenyl)-4,5-diphenylimidazole] (*o*-Cl-HABI; Fig. 1D) as a photoinhibitor. Whereas HABIs are well known as effective photoinitiators in the presence of complementary, hydrogen-donating co-initiators (19), in the absence of co-initiators, the lophyl radicals transiently generated upon HABI photolysis efficiently inhibit radical-mediated, chain-growth polymerization (fig. S1) by rapidly recombining with propagating, carbon-centered radicals and thus can be used to prevent polymerization adjacent to the illumination window.

Independently controlling initiation and inhibition necessitates that photoinitiating and photoinhibiting species have complementary absorbance spectra. As shown in Fig. 1E, *o*-Cl-HABI exhibits very weak absorbance in the blue region of the spectrum and moderate absorbance in the near ultraviolet (UV), complementing the absorbance spectrum of CQ that absorbs blue light ($\lambda_{\text{max}} = 470$ nm) but absorbs poorly in the near UV. This minimal overlap in the absorbance spectra of CQ

Copyright © 2019
The Authors, some
rights reserved;
exclusive licensee
American Association
for the Advancement
of Science. No claim to
original U.S. Government
Works. Distributed
under a Creative
Commons Attribution
NonCommercial
License 4.0 (CC BY-NC).

¹Department of Chemical Engineering, University of Michigan, Ann Arbor, MI 48109, USA. ²Macromolecular Science and Engineering Program, University of Michigan, Ann Arbor, MI 48109, USA. ³Department of Biomedical Engineering, University of Michigan, Ann Arbor, MI 48109, USA.

*These authors contributed equally to this work.

†Corresponding author. Email: maburns@umich.edu (M.A.B.); tfscott@umich.edu (T.F.S.)

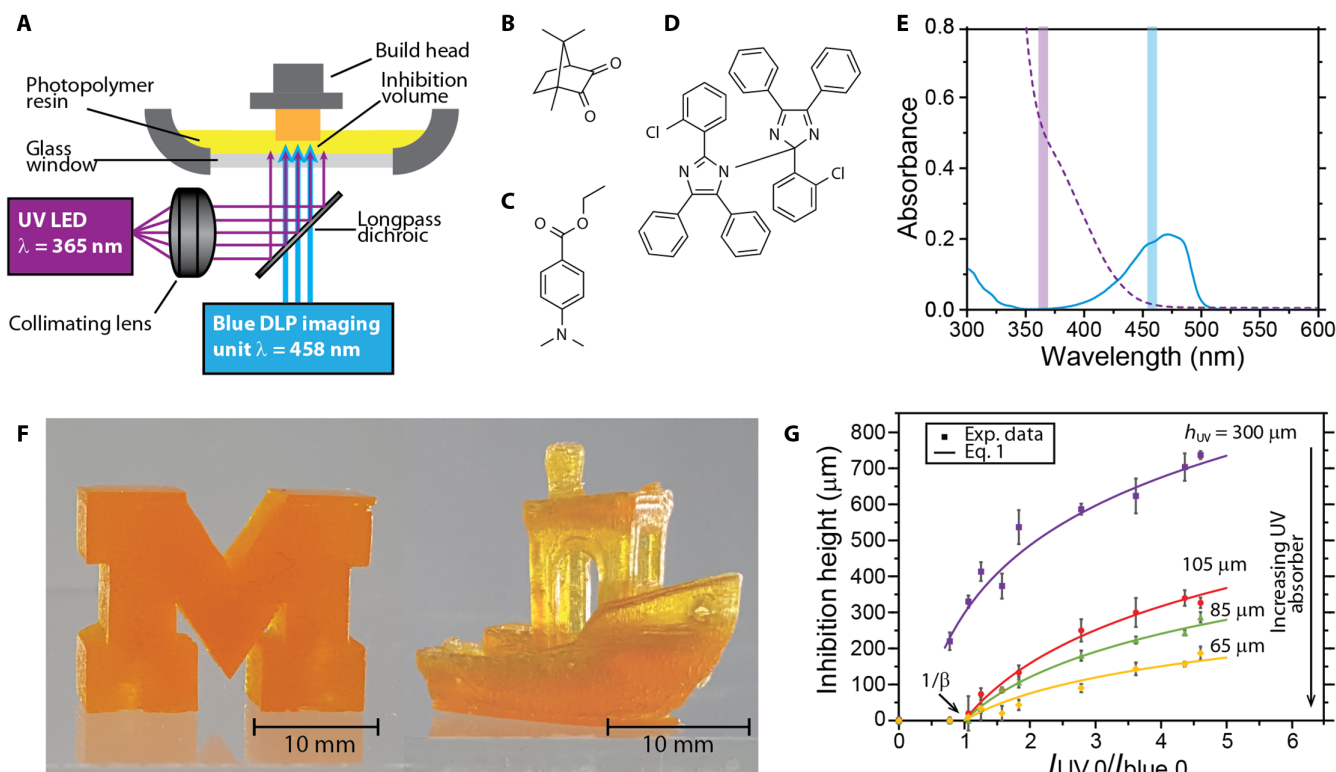


Fig. 1. Concurrent, two-color photoinitiation and photoinhibition. (A) Optical setup for two-color SLA by concurrent photopolymerization and photoinhibition. Near UV (365 nm) is superimposed onto patterned blue (458 nm) with a dichroic mirror and projected through a transparent window into a photopolymerizable resin vat. Structures of (B) photoinitiator CQ, (C) co-initiator EDAB, and (D) photoinhibitor *o*-Cl-HABI. (E) UV-visible spectra of CQ (solid blue line) and *o*-Cl-HABI (dashed violet line) in tetrahydrofuran (THF). The UV and blue wavelengths used by the two-color AM system are highlighted by the violet and blue vertical bars, respectively. (F) Solid block M (left) and tug boat [model detailed in (37)] (right) printed using the two-color photopolymerization/photoinhibition stereolithography system at 500 and 375 mm/hour, respectively. (G) The polymerization inhibition volume thickness is affected by varying intensity ratios of the incident irradiation wavelengths ($I_{UV,0}/I_{blue,0}$) and resin absorbance (h_{UV}).

and *o*-Cl-HABI in the near UV to blue region of the spectrum enables polymerization to be selectively initiated with blue light and inhibited with UV light.

The thickness of the polymerization inhibition volume can be controlled by varying the ratio of the intensities of the two illuminating light sources. When both UV and blue light are supplied to the resin, an inhibition volume with no polymerization is generated adjacent to the window. Above this region, polymerization occurs, allowing the continuous printing of objects, such as those shown in Fig. 1F, without deleterious window adhesion. The inhibition volume thickness (i.e., the vertical distance into the resin from the transparent window in which no polymerization occurs) is dependent on the incident initiating and inhibiting light intensities ($I_{blue,0}$ and $I_{UV,0}$, respectively) such that

$$\text{Inhibition volume thickness} = \frac{\log\left(\frac{\beta I_{UV,0}}{I_{blue,0}}\right)}{1/h_{UV} - 1/h_{blue}} \quad (1)$$

Here, the inhibition coefficient (β) is a constant for a given resin composition and incorporates the ratio of inhibitor to initiator absorbance cross sections, quantum yield, and reaction rate constants (20). The absorption height of a material, h_{UV} and h_{blue} , is defined as the inverse of the sum of the concentrations of all absorbing species (c_i) multiplied by their wavelength-specific absorptivity (ϵ_i) (i.e., $h_i = \frac{1}{\sum \epsilon_i c_i}$) and is

equal to the depth into an absorbing medium at which the light is 90% attenuated.

Figure 1G shows that inhibition volume thickness, calculated using a subtractive technique (15), is controlled by varying both the ratios of the incident radiation and the concentration of the UV absorber. Adjustment of $I_{UV,0}/I_{blue,0}$ changes the relative rates of initiating and inhibiting radical generation within the resin [trimethylolpropane triacrylate (TMPTA)] and can be used to control the inhibition thickness. Alternatively, the UV absorber concentration (Tinuvin 328; see fig. S3) can be changed to achieve a similar control over the inhibition volume thickness. Increasing the UV absorber concentration to decrease h_{UV} selectively confines UV light, and hence generation of inhibiting radicals, to progressively thinner regions above the projection window. It is important to note that a minimum intensity ratio at which initiation and inhibition rates are balanced is required to generate an inhibition volume and can be shown to equal $(I_{UV,0}/I_{blue,0})_{crit} = 1/\beta$ (see supplement 1). In this TMPTA-based system, $1/\beta$ is found to be approximately 1; nevertheless, this value is dependent on resin composition, necessitating experimental determination for specific resin formulations.

The thickness of this polymerization inhibition volume adjacent to the projection window is a critical parameter for continuous stereolithographic fabrication. Previously reported inhibition layers resulting from oxygen inhibition are typically only tens of micrometers thick (15, 16). Although this inhibition layer eliminates adhesion to the window, its

small thickness curtails resin reflow underneath the emergent object, especially in objects with large cross-sectional areas (21), and necessitates the use of low-viscosity resins or fabrication of objects with small cross sections. Here, the inhibition volume thickness can be modulated by altering the UV absorbance of the resin or varying the intensities of the initiating and inhibiting light sources such that inhibition volume thicknesses in the hundreds of micrometers are readily obtained. These thick inhibition volumes are particularly desirable when using viscous resin formulations, further expanding the monomer palette, or to allow resin reflow into the print area for objects with large cross-sectional areas. Nevertheless, increases in the inhibition volume thickness are typically accompanied by decreased polymerization rates, and hence slower print speeds, owing to attenuation of the initiation wavelength intensity within the resin bath. Notably, the system described here can negate this limitation and achieve equivalent polymerization rates for different inhibition volume thicknesses by accompanying any variation in the inhibition wavelength intensity with a corresponding initiation wavelength intensity change (see fig. S2).

Continuous AM

The large inhibition volume, in conjunction with high photoinitiation rates, facilitates continuous and rapid object printing. Notably, the high photoinitiation wavelength intensities that effect rapid polymerization rates also exacerbate separation and resin reflow issues in conventional and diffusion-reliant methods (15, 22). These high rates, though, can be used in this system because the inhibiting intensity can be adjusted to maintain a constant inhibition volume.

The maximum print speed for continuous printing in this system is a function of the absorption heights at the inhibiting and initiating wavelengths, h_{UV} and h_{blue} , the intensity of the initiating and inhibiting wavelengths ($I_{blue,0}$ here), and the amount of energy required to cure the resin, E_c , such that (see supplement 2)

$$\text{Max. print speed} \propto \frac{I_{blue,0} h_{blue} - \beta I_{UV,0} h_{UV}}{E_c} \quad (2)$$

Reducing the inhibition volume thickness by decreasing h_{UV} at constant irradiation intensity is predicted to increase print speeds as polymerization proceeds closer to the projection window, where limited blue light attenuation affords high initiation wavelength intensity. Practically, the theoretical maximum print speed is difficult to achieve owing to lingering inhibiting radicals, mechanical properties of the cured resin, and reflow limitations dictated by the resin viscosity. Nevertheless, we are able to print parts at speeds up to approximately 2 m/hour for the argyle structures shown in Fig. 2A.

In this system, the depth to which light penetrates and ultimately cures resin is controlled by modulating the resin's blue absorbance (Fig. 2B), with the cured thickness for a given irradiation dose of initiating light given by

$$\text{Cured thickness} = h_{blue} \log\left(\frac{I_{blue,0} t}{E_c}\right) \quad (3)$$

where $I_{blue,0} t$ (23) is the product of the irradiation intensity and time. At the slowest print speed, the apparent void percentage of the printed argyle structure exceeded that of the design (Fig. 2A), attributable to polymerization-induced shrinkage (24); however, deviation of the

printed part volumes from their design increased with raised print speed, primarily owing to unwanted polymerization beyond the designed feature (known as "cure through"). Although adding blue-absorbing

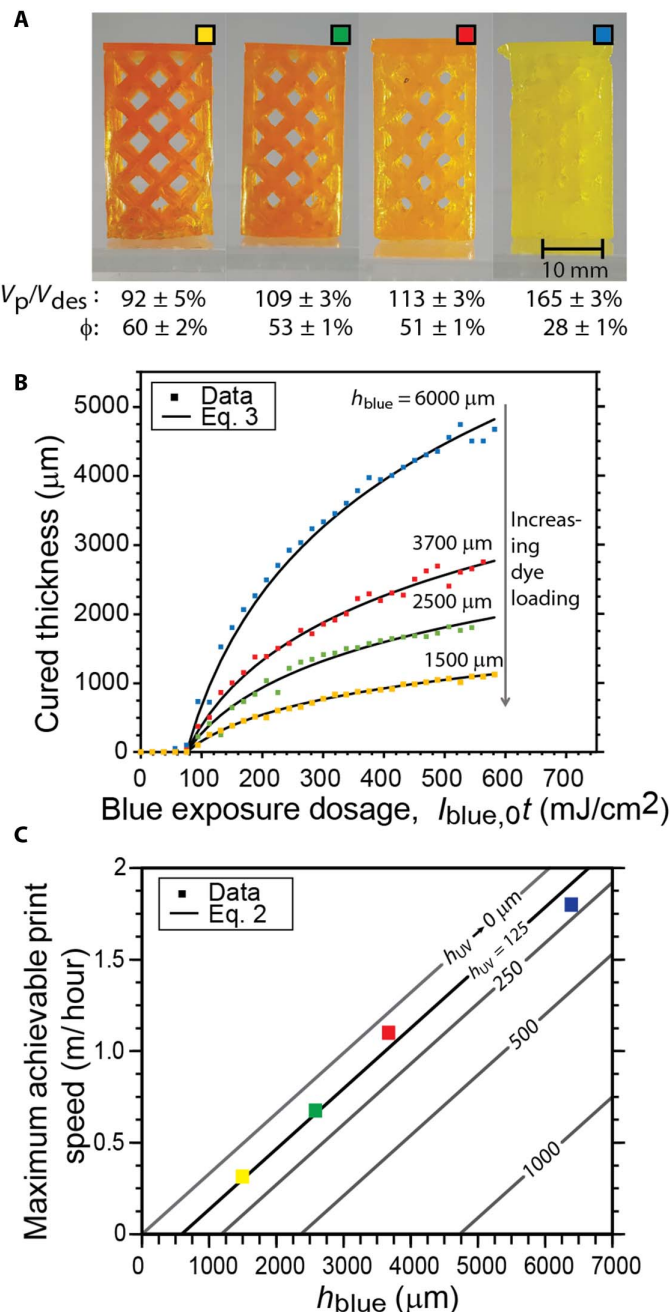


Fig. 2. Rapid, continuous AM with two-color photoinitiation and photoinhibition. (A) Argyle models printed using photoinhibition to enable continuous printing, with the percentage void (ϕ) and volume of the printed part (V_p) relative to the designed part (V_{des}) shown below each part. The designed void was $\phi = 57\%$. (B) Cured thickness versus dosage of blue light for four acrylate-based resin formulations prepared with varying blue-absorbing dye (Epilight 5675) loadings. (C) Maximum vertical print speeds achievable for varying blue absorbance heights. All printing was done with $I_{blue,0}$ of $110 \text{ mW}/\text{cm}^2$ and $I_{UV,0}$ of $130 \text{ mW}/\text{cm}^2$, with h_{UV} of $125 \mu\text{m}$. The influence of varying h_{UV} , and hence inhibition volume thickness, on the predicted maximum achievable print speed, as determined by Eq. 2, is shown as solid lines.

dyes (e.g., Epolight 5675; see fig. S3) can rectify this cure through effect to improve the fidelity of printed parts to their design, a compromise between vertical resolution and print speed exists in continuous AM systems (Fig. 2C), as has been previously reported (15). Print fidelity can also be improved by using resin formulations that exhibit inherently low polymerization shrinkage or by modifying the projected images to correct for shrinkage. Nevertheless, increasing the print speed at a constant dye loading results in decreased gel fractions of the completed part (see fig. S6) owing to lower light doses for faster-printed parts.

Hexaarylbiimidazoles as radical polymerization photoinhibitors

The concurrent photoinitiation and photoinhibition described here can be applied to a range of monomer classes for use in this AM sys-

tem. HABI's exhibit several attributes favoring their potential as universal photoinhibitors of radical-mediated, chain-growth polymerizations, including their favorable absorbance spectra and the inability of HABI-derived lophyl radicals to directly initiate polymerization of (meth)acrylates (25), greatly expanding the compatible monomer palette. To demonstrate the broad applicability of our photoinitiator/photoinhibitor system, acrylate, methacrylate, and vinyl ether/maleimide (i.e., electron donor and electron acceptor monomers) resins (see Fig. 3, A to E) formulated with CQ, EDAB, and *o*-Cl-HABI displayed rapid curing upon blue irradiation, suggesting that the HABI did not produce polymerization rate-retarding chain transfer reactions, and, while under exclusive near-UV irradiation, very limited to no curing was observed. Upon concurrent blue and near-UV irradiation, polymerization rates decreased precipitously relative to those observed under exclusively blue irradiation for all resin formulations examined, approaching zero for the

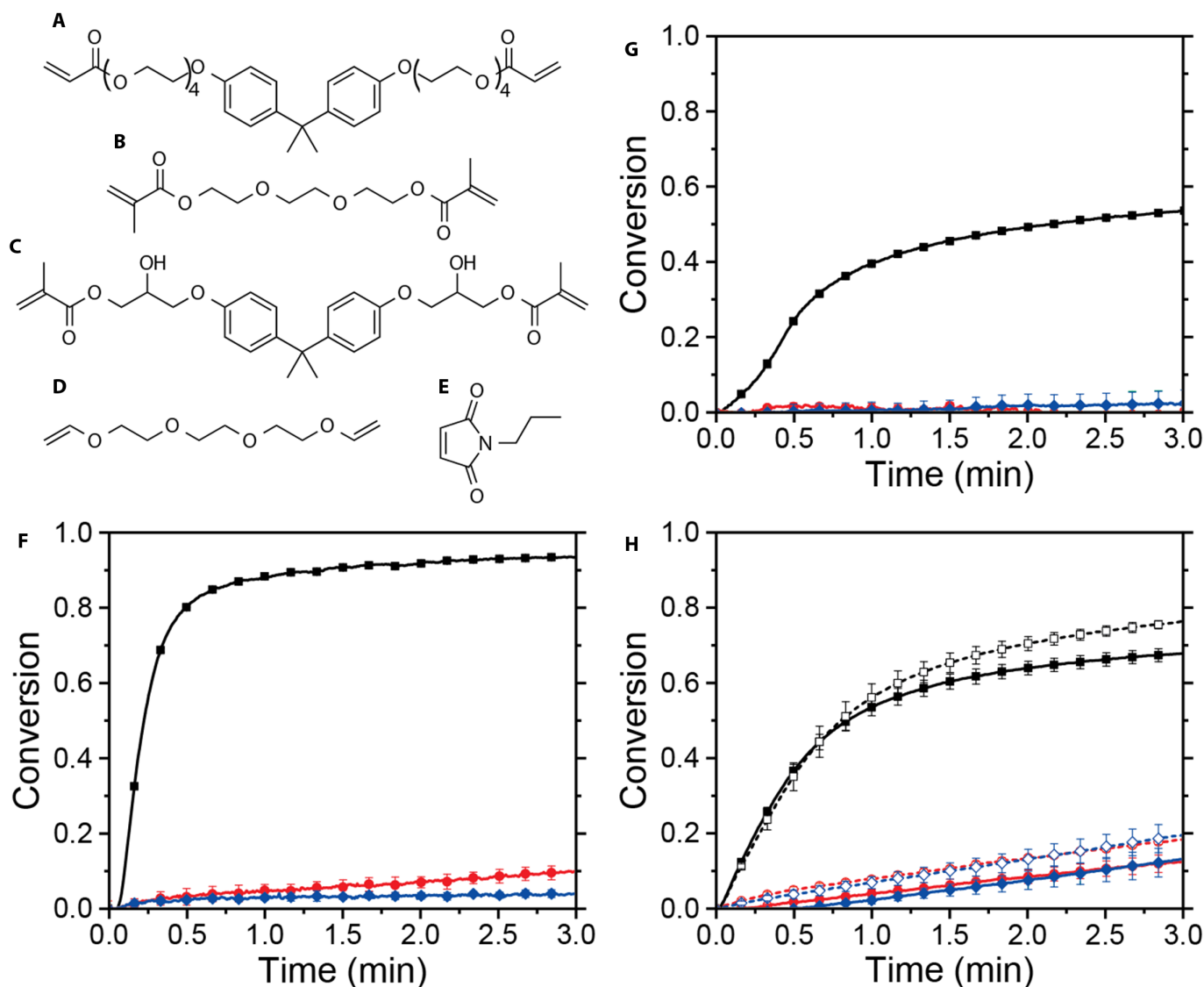


Fig. 3. Wavelength-selective photoinitiation and photoinhibition of radical-mediated, chain-growth photopolymerization. Monomers examined include (A) bisphenol A ethoxylate diacrylate (BPAEDA; $n = 4$), (B) triethylene glycol dimethacrylate (TEGDMA), (C) bisphenol A glycerolate dimethacrylate (bisGMA), (D) triethylene glycol divinyl ether (TEGDVE), and (E) *N*-(*n*-propyl)maleimide (NPM). Alkene conversion versus time for resin formulations of (F) BPAEDA, (G) bisGMA/TEGDMA, and (H) TEGDVE/NPM (vinyl ether and maleimide conversions denoted by solid and dashed lines, respectively) under continuous irradiation with exclusively 470 nm @ 100 mW/cm² (black line, squares), 470 nm @ 100 mW/cm² and 365 nm @ 30 mW/cm² (red line, circles), and 365 nm @ 30 mW/cm² (blue line, diamonds).

(meth)acrylates (Fig. 3, F to H). Note that other two-color irradiation schemes have been demonstrated previously for subdiffraction, direct-write photolithography (20, 26, 27). These systems used CQ and EDAB as a blue light photoinitiator system and tetraethylthiuram disulfide (TETD) as a UV-active photoinhibitor. Unfortunately, the utility of TETD in rapid AM is hindered by its participation in chain transfer reactions with propagating radical species (28), resulting in significantly reduced photopolymerization rates at raised TETD concentrations even under exclusively photoinitiating irradiation, while co-irradiation at the photoinhibition wavelength yields reduced polymerization rates but does not completely cease polymerization (20). Moreover, TETD has only been shown to effectively inhibit methacrylate resins, limiting the palette of compatible monomers.

Single-exposure surface topographical patterning

A significant and unique attribute of our system is that, by using the concurrent photoinitiation and photoinhibition in conjunction with spatially specific variation in light intensity, our system has the ability to produce complex 3D surface features with a single, two-color

exposure. Projecting blue images of variable intensities (i.e., varying the intensity on a pixel-by-pixel basis) against a constant UV background affords spatial variation of $I_{UV,0}/I_{blue,0}$, consequently varying the inhibition volume thickness according to Eq. 1. This modulation creates a complex 3D patterned inhibition volume and enables localized surface patterning of features, both of which are currently unattainable by contemporary methods.

Figure 4A shows a schematic of this procedure where the single-exposure topographical patterning was demonstrated with resin formulated with CQ/EDAB and *o*-Cl-HABI contained between two glass slides. The resin was exposed to a blue image of varying intensity, and this image was superimposed on a uniform, collimated UV light source (Fig. 4A). A single 10-s exposure yields cured features with a thickness variation of up to 700 μm and height differences as small as 125 μm (Fig. 4B); however, these magnitudes can be readily varied by adjusting the UV- and blue-absorbing dye loadings to refine the wavelength-dependent absorption characteristics of the resin (i.e., by adjusting h_{UV} and h_{blue}). The ability to use this technique to produce patterned features with 3D structures is demonstrated with a

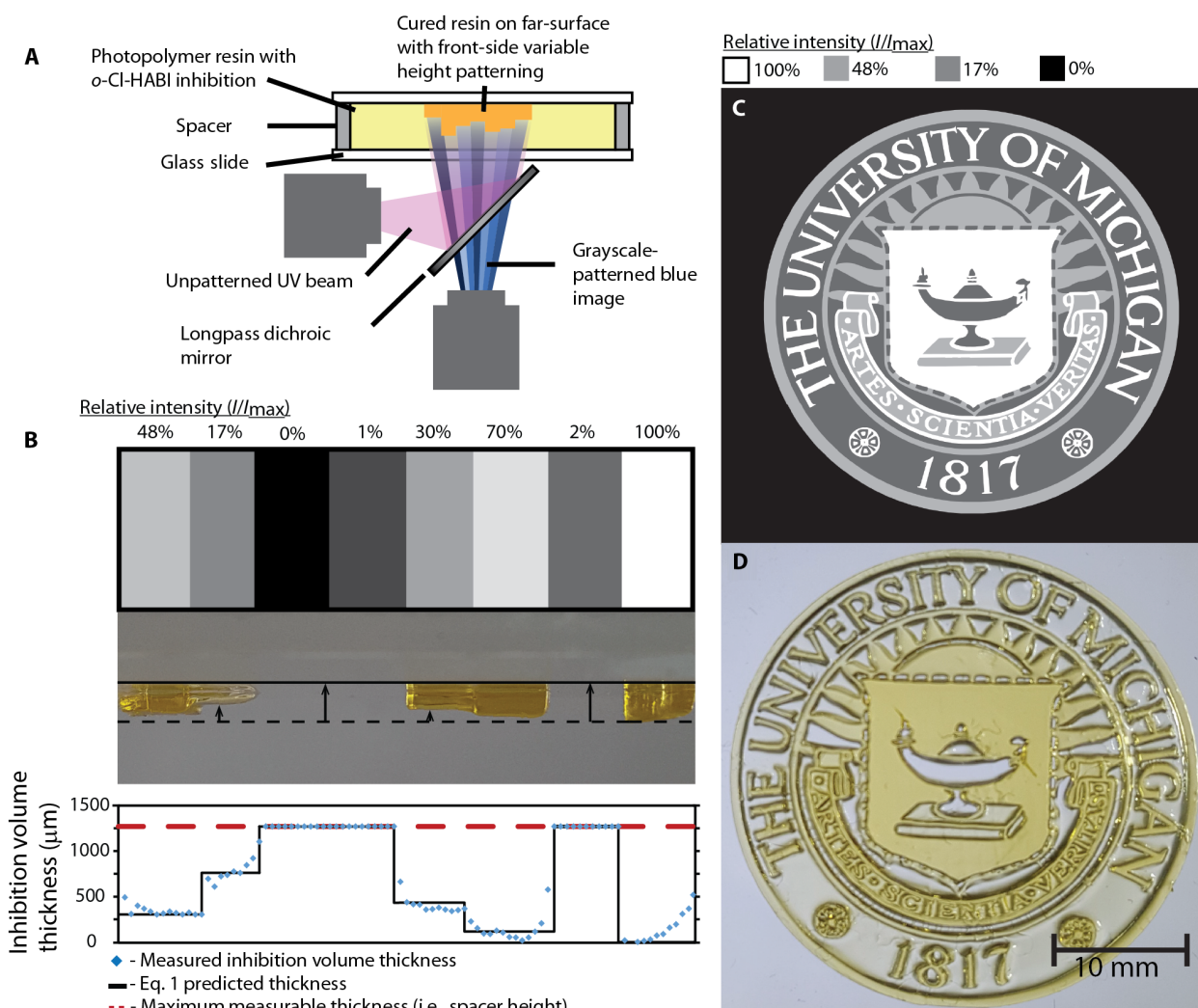


Fig. 4. Two-color photoinitiation and photoinhibition enable controllable, far-surface patterning of complex 3D structures. (A) Setup used for intensity-patterned printing. (B) Use of variable intensity images enables pixel-wise adjustment of $I_{UV,0}/I_{blue,0}$, producing variation in inhibition height and, therefore, printed part topography. (C) Four-level intensity image of the University of Michigan seal. (D) Variable thickness part produced by a single intensity-patterned exposure.

four-intensity-level image (Fig. 4C). The cured resin resulting from exposure to the image in Fig. 4C shows the expected variation in thickness (Fig. 4D), and the 200- μm text features are readily resolved.

DISCUSSION

The controllable, concurrent photoinitiation and photoinhibition used in this fabrication system have, in addition to high vertical print speeds, considerable advantages over contemporary approaches. By eliminating the need for thin, O_2 -permeable projection windows, this process has the potential to be scaled for rapid production of very large objects. Moreover, by dynamically controlling inhibition using this method, reflow into the inhibition volume during printing can be optimized to ameliorate reflow problems associated with production of large cross-sectional area parts, significantly broadening the applicability of AM for mass production. Using variable intensity irradiation with concurrent photoinitiation and photoinhibition allows single-step fabrication of cured materials with intricate surface topographies, enabling rapid generation of personalized products or overcoming numerous time-consuming steps currently used in microfabrication. The application of multiwavelength systems to SLA is a new direction in AM, where, in addition to the volumetric polymerization control described here, two-color systems designed to effect orthogonal reactions may enable fabrication of parts with localized variation of material and chemical properties (29).

MATERIALS AND METHODS

Triethylene glycol dimethacrylate (TEGDMA; Esstech Inc., Essington, PA) and bisphenol A glycidyl methacrylate (bisGMA, Esstech) were formulated as a mixture consisting of 50 weight % (wt %) TEGDMA and 50 wt % bisGMA. *N*-(*n*-propyl)maleimide (NPM; Alfa Aesar, Haverhill, MA) and triethylene glycol divinyl ether (TEGDVE; Sigma-Aldrich, St. Louis, MO) were formulated as a mixture such that the maleimide and vinyl ether functional groups were present at a 1:1 stoichiometric ratio. Bisphenol A ethoxylate diacrylate, EO/phenol 4.0 (BPAEDA; Sigma-Aldrich) was used without comonomers. (\pm)-Camphorquinone CQ; (Esstech) was used as a blue light-active photoinitiator in conjunction with ethyl 4-(dimethylamino)benzoate (EDAB; Esstech) as a co-initiator at the concentrations indicated. 2,2'-Bis(2-chlorophenyl)-4,4',5,5'-tetraphenyl-1,2'-biimidazole (*o*-Cl-HABI, TCI America, Portland, OR) was used as a photoinhibitor at the concentrations indicated. Owing to poor solubility of *o*-Cl-HABI in the monomers, *o*-Cl-HABI was dissolved in tetrahydrofuran (THF; containing 0.025% butylated hydroxytoluene as preservative; Fisher Scientific, Hampton, NH) as a ~30 wt % solution before formulating the resins. The bisGMA/TEGDMA monomer mixture was formulated with 0.2 wt % CQ, 0.5 wt % EDAB, and 3 wt % *o*-Cl-HABI. BPAEDA was formulated with 0.2 wt % CQ, 0.5 wt % EDAB, and 2 wt % *o*-Cl-HABI. The TEGDVE/NPM monomer mixture was formulated with 1.0 wt % CQ, 0.5 wt % EDAB, and 5 wt % *o*-Cl-HABI. All monomer quantities were adjusted to account for the THF, in which *o*-Cl-HABI was dissolved. For the *o*-Cl-HABI photoinitiation testing, bisGMA/TEGDMA was formulated with 1 wt % *o*-Cl-HABI and either no co-initiator or 0.5 wt % of either EDAB or 2-mercaptobenzothiazole (MBT, Sigma-Aldrich).

Photopolymerizable resins for 3D printing were prepared with a 1/0.5/3 wt % mixture of CQ, EDAB, and *o*-Cl-HABI, respectively. Inhibition volume thickness tests were exclusively conducted with TMPTA (Alfa Aesar) as monomer. Resins used for continuous 3D

printing and varying intensity printing were mixtures of monomers, oligomers, and reactive diluents, including TMPTA, TEGDMA, 1,6-hexanediol diacrylate (TCI America, Portland, OR), Sartomer CN2920 (Sartomer, Exton, PA), Sartomer CN981 (Sartomer), and isobornyl acrylate (TCI America). Tinuvin 328 (BASF, Florham Park, NJ) was used as a UV absorber, and Epolight 5675 (Epolin, Newark, NJ) was used as a blue light absorber. All chemicals were used as received. All polymerizations were conducted at room temperature.

UV-visible spectrophotometry

UV-visible spectrophotometry was performed on 1 wt % solutions of *o*-Cl-HABI and CQ in THF and 1.1×10^{-4} M Tinuvin 328 and Epolight 5675 (1×10^{-2} g/liter) in isopropyl alcohol using an Agilent Technologies Cary 60 UV-Vis spectrophotometer. Spectra were collected from 200 to 800 nm, with 1-nm spacing on solutions using a 1-mm path length quartz cuvette in the dark.

FTIR spectroscopy

Blue light was provided by a collimated, light-emitting diode (LED)-based illumination source (Thorlabs M470L3-C1) with an emittance centered at 470 nm (full width at half maximum, 25 nm), used in combination with a current-adjustable LED driver (Thorlabs LEDD1B) for intensity control. UV light was provided by a UV spot curing system (OmniCure LX500, Excelitas Technologies) equipped with an OmniCure LED MAX head with an emittance centered at 365 nm. Irradiation intensities were measured with an International Light IL1400A radiometer equipped with a GaAsP detector (model SEL005), a 10 \times attenuation neutral density filter (model QNDS1), and a quartz diffuser (model W).

Resin formulations were introduced between NaCl crystal windows (International Crystal Laboratories) separated by spacers (26 μm thick for bisGMA/TEGDMA, 51 μm thick for BPAEDA, and 13 μm thick for NPM/TEGDVE to maintain constant sample thickness during polymerization). Each sample was placed in a Thermo Scientific Nicolet 6700 Fourier transform infrared (FTIR) spectrometer equipped with a horizontal transmission accessory, as described previously (30), and spectra were collected from 650 to 4000 cm^{-1} at a rate of 2 per second. The functional group conversion upon irradiation was determined by monitoring the disappearance of the peak area centered at 1635 cm^{-1} for the methacrylate stretch, 1636 cm^{-1} for the acrylate stretch, 1618 cm^{-1} for the vinyl ether stretch, and 829 cm^{-1} for the maleimide C=C double bond stretch. The respective sample thicknesses for the formulations were chosen to ensure that the functional group peaks remained within the linear regime of the instrument detector while affording good signal-to-noise ratio and maintaining optically thin and isothermal polymerization conditions. All experiments were performed in triplicate, and the photoinitiator and photoinhibitor concentrations and irradiation intensities were as indicated in Materials and Methods and figure legends.

Inhibition volume thickness measurements

UV light from a high-powered LED ($\lambda_{\text{max}} = 365$ nm, 1400 mA, Thorlabs #M365LP1) was collimated using an aspheric condenser lens [$\text{Ø}2''$; $f = 32$ mm; numerical aperture (NA), 0.76; Thorlabs, ACL50832U] and focused with an adjustable collimation adapter (Thorlabs, SM2F). Optical components were held in place with a 60-mm cage cube system (Thorlabs, LC6W). A high-powered blue LED ($\lambda_{\text{max}} = 458$ nm, $I_{\text{F}} = 1400$ mA, Osram LE B Q7WP-5C8C-24) was retrofitted into a commercial DLP projector (Optoma ML750). Light from the blue projection system passed through a biconvex ($\text{Ø}2''$; $f = 100$ mm; NA, 0.76; Thorlabs, LB1630) lens to reduce the focal distance and

superimposed with the UV light using a longpass dichroic mirror ($\text{\O}2''$, 425-nm cutoff; Thorlabs, DMLP425L). The UV LED was driven by a BuckPuck LED driver ($I = 1000$ mA; LEDdynamics Inc., 3023-D-E-1000), and the blue LED was driven by a constant current power supply (10,000 mA, Mean Well HLG-120H-12B). The intensity of the LEDs was controlled using a custom LabVIEW virtual instrument (VI) that output a 0- to 5-V analog signal, which adjusted the current from the LED driver. Light intensity at a given voltage was calibrated by using an International Light IL1400A radiometer. 3D printed (Markforged Mark II, Nylon) spacers (800 μm thick) were affixed to a glass slide using an epoxy adhesive to create a well for the photopolymer. Resin was pipetted into the well and sealed with another glass slide. The resin was then cured for 10 s at $I_{\text{blue}} = 78.5$ mW/cm² under varying UV irradiation intensities to give $0 < I_{\text{UV}}/I_{\text{blue}} < 2$. The cured resin was rinsed using isopropanol and reexposed to blue light for an additional minute to complete curing. The thickness of the cured part was measured with a micrometer. The thickness of the inhibition volume was then calculated from $h_{\text{IV}} = h_{\text{s}} - h_{\text{c}}$, where h_{IV} , h_{s} , and h_{c} are the thicknesses of the inhibition volume, spacer, and cured plug, respectively.

Continuous 3D printing

A custom build head was designed using Autodesk Fusion 360 and fabricated out of nylon using 3D printing (Markforged Mark II). A metal base plate was attached at the base of the build head using two wingnuts. The build head was attached to a commercially available linear screw actuator (Rattmmotor CBX1605-300A) to enable vertical motion. Motion was controlled using an on/off digital signal from a custom LabVIEW VI to start/stop a signal from a signal generator (Agilent 33220A).

Models were designed using DesignSpark Mechanical 2.0 or Autodesk Fusion 360 and exported as STL files. Image slices were created from STL files using the slicing feature in Autodesk Netfabb 2017. All models were sliced using a slice height of 25 μm to ensure a short slicing time while maintaining good feature resolution. During printing, image slices were displayed concurrently with movement of the build head using a LabVIEW VI (see fig. S5). Parts were rinsed with isopropanol after printing to remove uncured resin.

Gas pycnometry

A gas pycnometer (MVP-60C, Quantachrome Instruments) was used to measure the volume of 3D printed parts. Each sample mass was placed in a cylindrical sample cell and pressurized with helium gas. The release of pressure resulted in the volume expansion of helium gas, which was converted to volume of the sample.

Determination of gel fraction

Samples prepared through continuous 3D printing were dried in the dark at 60°C for 24 hours and weighed. The samples were then extracted with THF for 24 hours using a Soxhlet apparatus, dried again at 60°C for 24 hours, and weighed to determine lost mass.

SUPPLEMENTARY MATERIALS

Supplementary material for this article is available at <http://advances.sciencemag.org/cgi/content/full/5/1/eaau8723/DC1>

Supplement 1: Derivation of Eq. 1

Supplement 2: Derivation of Eq. 2

Fig. S1. Wavelength-selective photoinitiation and transient photoinhibition of methacrylate polymerization.

Fig. S2. Effect of incident UV and blue illumination intensities on inhibition volume thickness and polymerization rate.

Fig. S3. UV-vis spectra of UV and blue light absorbers.

Fig. S4. Influence of co-initiator on o-Cl-HABI photoinitiation.

Fig. S5. LabVIEW 2014 VI block diagram.

Fig. S6. Effect of print speed on the gel fraction of printed parts.

REFERENCES AND NOTES

- H. Lipson, M. Kurman, *Fabricated: The New World of 3D Printing* (John Wiley & Sons, 2013).
- S. H. Huang, P. Liu, A. Mokasdar, L. Hou, Additive manufacturing and its societal impact: A literature review. *Int. J. Adv. Manuf. Technol.* **67**, 1191–1203 (2013).
- C. L. Ventola, Medical applications for 3D printing: Current and projected uses. *Pharm Ther.* **39**, 704–711 (2014).
- H. N. Chia, B. M. Wu, Recent advances in 3D printing of biomaterials. *J. Biol. Eng.* **9**, 4 (2015).
- Q. Liu, M. C. Leu, S. M. Schmitt, Rapid prototyping in dentistry: Technology and application. *Int. J. Adv. Manuf. Technol.* **29**, 317–335 (2006).
- T. Wohlers, T. Caffrey, Additive manufacturing: Going mainstream. *Manuf. Eng.* **150**, 67–73 (2013).
- J. Manyika, M. Chui, J. Bughin, R. Dobbs, P. Bisson, A. Marrs, *Disruptive Technologies: Advances That Will Transform Life, Business, and the Global Economy* (McKinsey Global Institute, 2013).
- K. Takagishi, S. Umez, Development of the improving process for the 3D printed structure. *Sci. Rep.* **7**, 39852 (2017).
- H. Chen, X. Yang, L. Chen, Y. Wang, Y. Sun, Application of FDM three-dimensional printing technology in the digital manufacture of custom edentulous mandible trays. *Sci. Rep.* **6**, 19207 (2016).
- J. T. Belter, A. M. Dollar, Strengthening of 3D printed fused deposition manufactured parts using the fill compositing technique. *PLOS ONE* **10**, e0122915 (2015).
- W. E. Frazier, Metal additive manufacturing: A review. *J. Mater. Eng. Perform.* **23**, 1917–1928 (2014).
- W. Gao, Y. Zhang, D. Ramanujan, K. Ramani, Y. Chen, C. B. Williams, C. C. L. Wang, Y. C. Shin, S. Zhang, P. D. Zavattieri, The status, challenges, and future of additive manufacturing in engineering. *Comput. Aided Des.* **69**, 65–89 (2015).
- C. Sun, N. Fang, D. M. Wu, X. Zhang, Projection micro-stereolithography using digital micro-mirror dynamic mask. *Sens. Actuators A Phys.* **121**, 113–120 (2005).
- A. Bertsch, J. Y. Jézéquel, J. C. André, Study of the spatial resolution of a new 3D microfabrication process: The microstereolithography using a dynamic mask-generator technique. *J. Photochem. Photobiol. Chem.* **107**, 275–281 (1997).
- J. R. Tumbleston, D. Shirvanyants, N. Ermoshkin, R. Januszewicz, A. R. Johnson, D. Kelly, K. Chen, R. Pinschmidt, J. P. Rolland, A. Ermoshkin, E. T. Samulski, J. M. DeSimone, Continuous liquid interface production of 3D objects. *Science* **347**, 1349–1352 (2015).
- R. Januszewicz, J. R. Tumbleston, A. L. Quintanilla, S. J. Mecham, J. M. DeSimone, Layerless fabrication with continuous liquid interface production. *Proc. Natl. Acad. Sci. U.S.A.* **113**, 11703–11708 (2016).
- W. Zhu, K. R. Tringale, S. A. Woller, S. You, S. Johnson, H. Shen, J. Schimmelman, M. Whitney, J. Steinauer, W. Xu, T. L. Yaksh, Q. T. Nguyen, S. Chen, Rapid continuous 3D printing of customizable peripheral nerve guidance conduits. *Mater. Today* **21**, 951–959 (2018).
- J. G. Leprince, W. M. Palin, M. A. Hadis, J. Devaux, G. Leloup, Progress in dimethacrylate-based dental composite technology and curing efficiency. *Dent. Mater.* **29**, 139–156 (2013).
- B. M. Monroe, G. C. Weed, Photoinitiators for free-radical-initiated photoinitiation systems. *Chem. Rev.* **93**, 435–448 (1993).
- T. F. Scott, B. A. Kowalski, A. C. Sullivan, C. N. Bowman, R. R. McLeod, Two-Color Single-photon photoinitiation and photoinhibition for subdiffraction photolithography. *Science* **324**, 913–917 (2009).
- Y. Zhang, F. Zhang, Z. Yan, Q. Ma, X. Li, Y. Huang, J. A. Rogers, Printing, folding and assembly methods for forming 3D mesostructures in advanced materials. *Nat. Rev. Mater.* **2**, 17019 (2017).
- Y. Pan, H. He, J. Xu, A. Feinerman, Study of separation force in constrained surface projection stereolithography. *Rapid Prototyp. J.* **23**, 353–361 (2017).
- B. C. Gross, J. L. Erkal, S. Y. Lockwood, C. Chen, D. M. Spence, Evaluation of 3D printing and its potential impact on biotechnology and the chemical sciences. *Anal. Chem.* **86**, 3240–3253 (2014).
- J.-W. Park, G.-S. Shim, J.-H. Back, H.-J. Kim, S. Shin, T.-S. Hwang, Characteristic shrinkage evaluation of photocurable materials. *Polym. Test.* **56**, 344–353 (2016).
- X. Allonas, H. Obeid, J.-P. Fouassier, M. Kaji, Y. Ichihashi, Y. Murakami, Photochemistry and polymerization efficiency of bis-imidazole based photoinitiator systems. *J. Photopolym. Sci. Technol.* **16**, 123–128 (2003).

26. J. Fischer, M. Wegener, Three-dimensional optical laser lithography beyond the diffraction limit. *Laser Photon. Rev.* **7**, 22–44 (2012).
27. Z. Gan, Y. Cao, R. A. Evans, M. Gu, Three-dimensional deep sub-diffraction optical beam lithography with 9 nm feature size. *Nat. Commun.* **4**, 2061 (2013).
28. L. G. Lovell, B. J. Elliott, J. R. Brown, C. N. Bowman, The effect of wavelength on the polymerization of multi (meth) acrylates with disulfide/benzilketone combinations. *Polymer* **42**, 421–429 (2001).
29. N. D. Dolinski, Z. A. Page, E. B. Callaway, F. Eisenreich, R. V. Garcia, R. Chavez, D. P. Bothman, S. Hecht, F. W. Zok, C. J. Hawker, Solution mask liquid lithography (SMaLL) for one-step, multimaterial 3D printing. *Adv. Mater.* **30**, 1800364 (2018).
30. D. Ahn, S. S. Sathe, B. H. Clarkson, T. F. Scott, Hexaarylbisimidazoles as visible light thiol–ene photoinitiators. *Dent. Mater.* **31**, 1075–1089 (2015).
31. M. Ko, H. Kang, J. Kim, Y. Lee, J.-E. Hwang, How to measure quality of affordable 3D printing: Cultivating quantitative index in the user community. *Commun. Comput. Inf. Sci.* **617**, 116–121 (2016).

Acknowledgments: We thank the Stansbury group and P. Shah at the University of Colorado for their assistance with volumetric characterization by gas pycnometry. **Funding:** This work was supported by 3M Nontenured Faculty Award (to T.F.S.), T. C. Chang Professorship (to M.A.B.), University of Michigan Honor Society of Phi Kappa Phi Project Grant

(to H.L.v.d.L.), PPG Summer Fellowship Award (to H.L.v.d.L.), University of Michigan Rackham Graduate Student Research Grant (M.P.d.B.), and the NIH (NIDCR U01 DE023771).

Author contributions: M.P.d.B. and T.F.S. conceived the project. M.P.d.B., H.L.v.d.L., M.A.C., and R.J.W. designed and performed the experiments. M.A.B. and T.F.S. directed the project. M.P.d.B., H.L.v.d.L., M.A.C., M.A.B., and T.F.S. wrote the manuscript.

Competing interests: H.L.v.d.L., M.A.C., and T.F.S. are inventors on a patent application related to this work filed by the University of Michigan (no. 62/632,834, filed on 20 February 2018). All authors declare that they have no other competing interests.

Data and materials availability: All data needed to evaluate the conclusions in the paper are present in the paper and/or the Supplementary Materials. Additional data related to this paper may be requested from the authors.

Submitted 23 July 2018

Accepted 30 November 2018

Published 11 January 2019

10.1126/sciadv.aau8723

Citation: M. P. de Beer, H. L. van der Laan, M. A. Cole, R. J. Whelan, M. A. Burns, T. F. Scott, Rapid, continuous additive manufacturing by volumetric polymerization inhibition patterning. *Sci. Adv.* **5**, eaau8723 (2019).